REDUCED BRACE SECTION (RXS) PROOF OF CONCEPT: PHASE 1B

By
Santiago Bonetti
W.M. Kim Roddis
and
Adolfo Matamoros

A Report on Research Sponsored in Part by Butler Heavy Structures

Structural Engineering and Engineering Materials
SM Report No. 81

THE UNIVERSITY OF KANSAS CENTER FOR RESEARCH, INC.
2385 Irving Hill Drive – Campus West, Lawrence, Kansas 66045-7563

January 2006

Abstract

This report presents the results from the second phase of a proof-of-concept series of tests of the reduced braced section (RXS) system. This system is intended to provide a cost-effective alternative for the design of Concentrically Braced Frames (CBFs) under earthquake loads. The second test investigated the behavior of the RXS system under cyclic loading.

The hysteretic behavior of the specimen indicated that the behavior of the RXS system was sensitive to the eccentricity of the load imposed on the brace. Eccentric loading caused premature local bucking of the reduced section, which reduced the ability of the system to dissipate energy under repeated load reversals into the nonlinear range of response.

The behavior observed during the test shows that local buckling is a mode of failure that must be prevented in this type of system because of its adverse effect on the ability of the system to dissipate energy. Also, the design of the system must take into account a minimum eccentricity of the load transmitted to the brace at the brace-frame connection.

An alternative to improve the behavior of the system under repeated load reversals is to reinforce the reduced section in order to increase the local bucking load. **This report includes the applicable information specified in TEST REPORTING REQUIREMENTS [AISC, 2002, S9].**

Acknowledgements

This report is based on research performed by Santiago Bonetti at the Structural Engineering Laboratory, University of Kansas. Funding for this research was provided by Buttler Heavy Structures and the Department of Civil, Environmental, and Architectural Engineering at the University of Kansas.

Collaboration from Jim Weaver in the fabrication of the reaction frame is gratefully acknowledged.

Table of contents

List of Figures

List of Tables

Chapter 1 Introduction

The inelastic response of concentrically braced frames under seismic loads is dominated by the hysteretic behavior of the brace. For this reason the modeling of brace behavior when subjected to axial load reversals should be accurate and fully understood in order to effectively design concentrically braced frames.

The local behavior of round steel brace members with a reduced cross section area (RXS) subjected to load reversals is investigated through experimental and computational analyses as part of a series of proof-of-concept tests.

The main objective of this study is to develop a new method of design and construction of Concentrically Braced Frames, in accordance with the current steel seismic design provisions, that would provide a cost-effective improvement in the performance of this type of lateral-load-resisting system.

This report presents the second part to “Phase 1a/ RXS proof-of-concept”. The RXS system, and test specimen design calculations were presented in the report describing “Phase 1a”, in addition to results from the monotonic tension and monotonic compression load tests. For this reason, details of the system and prior tests are excluded from this report. In the second phase study, the local behavior of the reduced brace section under cyclic loading was investigated.

The test specimen, experimental configuration, equipment used, instrumentation, loading history, results and conclusions from the cyclic loading test “Phase 1b” are presented in the following pages.

Chapter 2 Experimental Plan

The behavior of the RXS system under cycling loading was evaluated experimentally to investigate the viability of the proposed structural system. The test was carried out at the Structural Engineering Laboratory at The University of Kansas. The specimen tested was made of HSS 6.625x0.250 A500 Grade B steel, same size and material type used for the two specimens tested in phase 1a.

2.1 Testing Fixtures

Test specimen fabrication initially used normal building fabrication practice with no special requirements for smooth edges cuts, but due to the mode of failure of the RXS system observed during phase 1a under monotonic tension (fracture initiated at the edge of the cut), normal bridge fabrication practice with smooth edge requirements was implemented for the cyclic loading test. The goal of improving fabrication of the specimen was to delay failure due to fracture and consequently improve the RXS hysteretic behavior.

The end fixtures were similar to those used in phase 1a. In phase 1b the 1 ½" A490 bolts were replaced by 6 feet and 3.5 feet ASTM A193 threaded steel rods in order to attach the test specimen to the self-reacting frame fabricated for the test. The specimen details are shown in Fig.1.

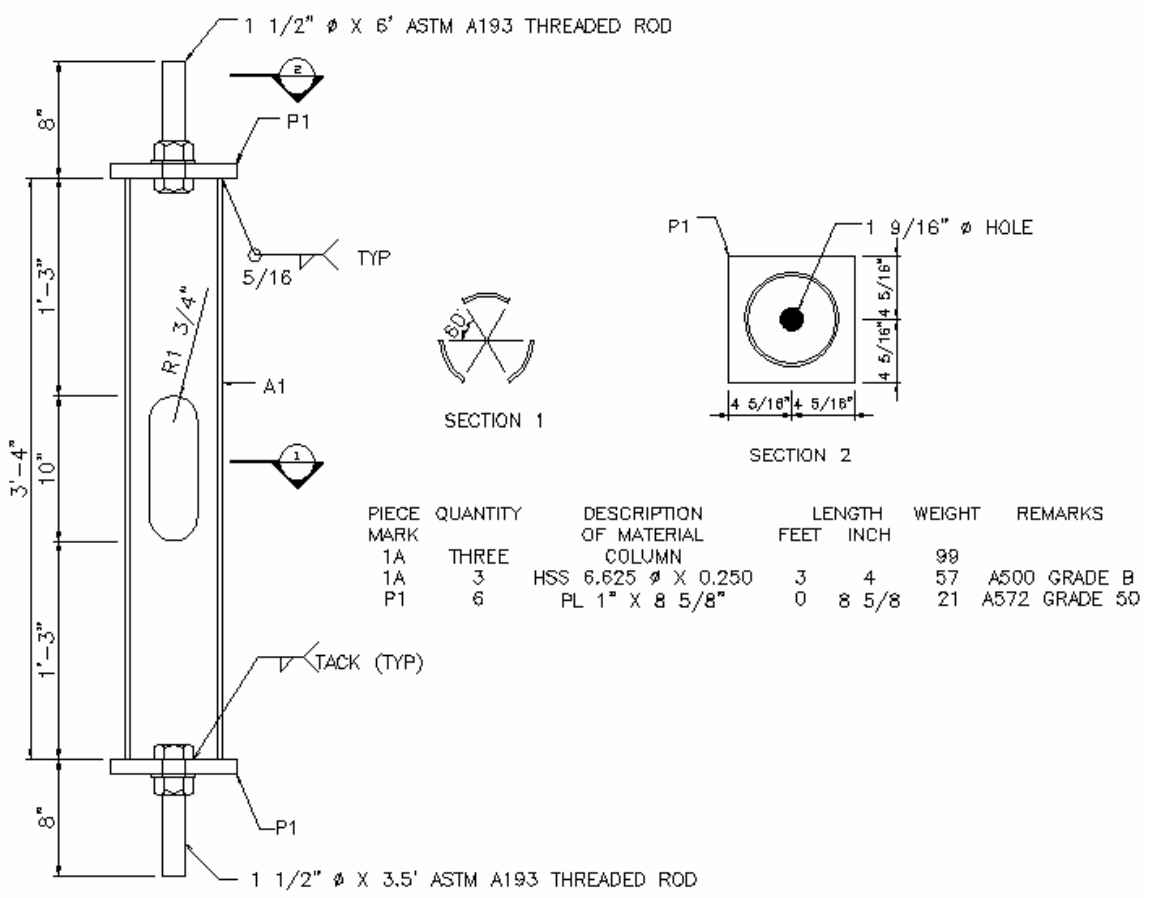

PIECE MARK	QUANTITY	DESCRIPTION OF MATERIAL	LENGTH FEET	LENGTH INCH	WEIGHT	REMARKS
1A	THREE	COLUMN			99	
1A	3	HSS 6.625 ø X 0.250	3	4	57	A500 GRADE B
P1	6	PL 1" X 8 5/8"	0	8 5/8	21	A572 GRADE 50

FIG. 1 – CYCLIC LOADING TEST SPECIMEN

2.2 Instrumentation

2.2.1 LVDTs:

LVDTs (Linear Variable Displacement Transformers) were used to measure linear displacement. They consist of a hollow cylindrical inductor body and a displaceable core that translates within the LVDT body so that the output voltage varies as the core moves. This variation in voltage is linear over a specific range, and is related to a linear displacement through a scale factor based on the slope of output voltage vs. linear displacement plot.

2.2.2 Strain Gages:

Bondable strain gages adhered to the outer surface of the test specimen measured strain at specific locations across the RXS. Strain gage locations are shown in Fig. 2. Three strain gages were equally placed along each arm. At the non-reduced sections, strain gage locations were located near the arm ends, in line with gages along the arms. Two strain gages were located in line with an oval cutout.

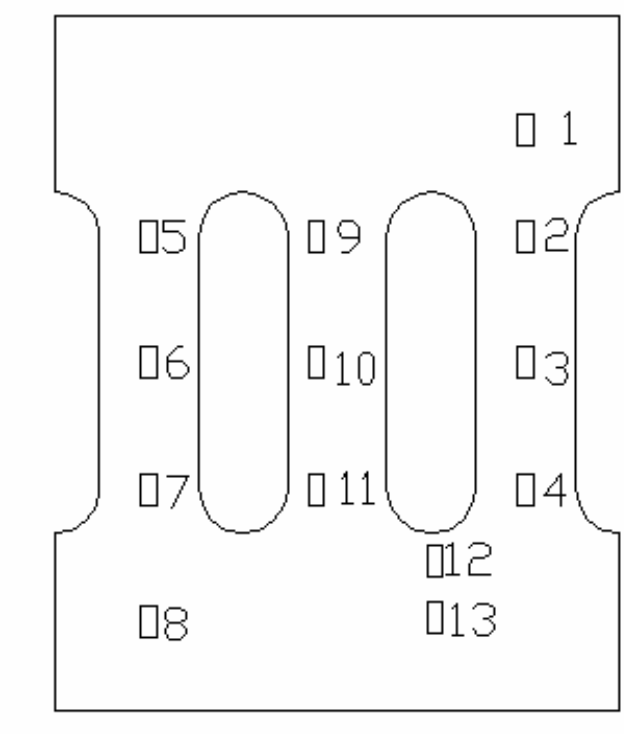

FIG. 2 - STRAIN GAGE LOCATIONS ON MONOTONIC TENSION SPECIMEN.

2.2.3 Whitewash:

A thin coat of whitewash, a mixture of Type S masonry lime and tap water, was applied to the test specimen. Whitewash provided a brittle coating with a high color contrast useful in revealing local yielding of the underlying bare steel, as the light colored brittle whitewash (and any brittle mill scale) detaches from the specimen surface. The

mixture, applied using different types of common paintbrushes, has a watery paint consistency and translucency during application, drying to opacity.

2.2.4 Load Cell:

Load cells were fabricated to measure the load applied to the brace. These load cells consisted of small metal hollow cylinders with four strain gages located around the outer surface of the cylinder connected to form a full Wheatstone bridge circuit. A Wheatstone bride is a divided bridge circuit with four active arms built by connecting the four strain gages (resistors) together in a diamond orientation (Fig. 3), these resistors are arranged so that the electric circuit is split into two paths.

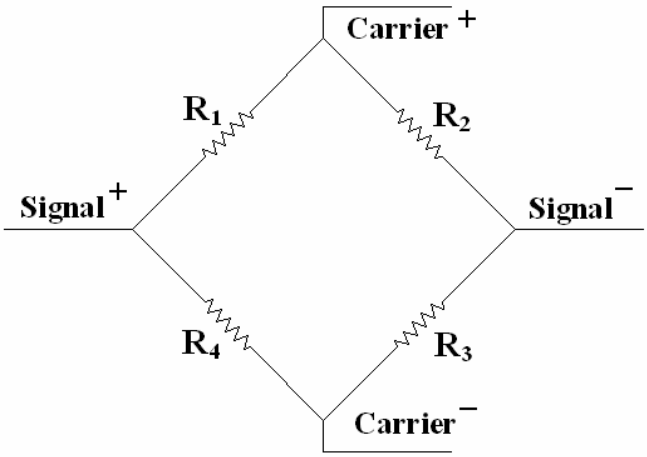

FIG. 3 - FULL WHEATSTONE BRIDGE ELECTRIC CIRCUIT.

When force is applied to the cylinder the output voltage from the full bridge circuit varies as the cylinder is subjected to compressive strains. This variation in voltage is linear over a specific range depending on the calibration, and it was related to linear force through a scale factor based on the slope of output voltage vs. linear force plot. The location of the strain gages and the wire distribution used to build the full Wheatstone

bridge circuit around the hollow cylinder is graphically described by unfolding the cylinder outer surface to an equivalent plate as shown in Fig. 4.

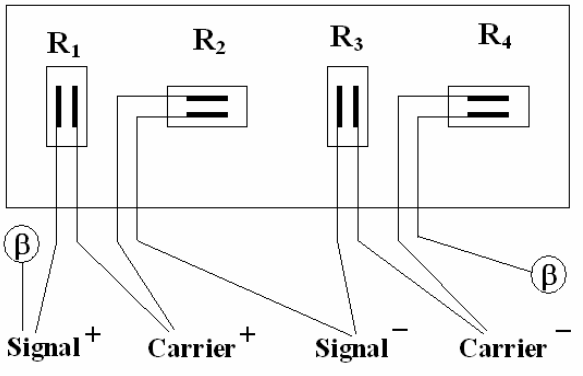

FIG. 4 - FULL WHEATSTONE BRIDGE CONFIGURATION.

2.2.5 Pressure transducer

One pressure transducer was used to measure load directly from the hydraulic hollow cylinders as a backup system for the handmade load cells. The pressure transducer was attached to the line originating from the hydraulic jack. Changes in pressure in the hydraulic line cause the output voltage from the pressure transducer to vary. This variation in voltage is linear over a specific range, and is related to the hydraulic pressure through a scale factor obtained from the slope of the output voltage vs. pressure curve, or directly related to the load by the slope of the output voltage vs. load calibration graph.

2.3 Loading Equipment and Data Acquisition

2.3.1 Data Acquisition System:

The data acquisition system was a Hewlett Packard (HP) VXI Plug and Play system operating in conjunction with a Dell 100 MHz Pentium II personal computer and

the HP DAC Express version 1.0 data acquisition software. The data acquisition system was configured to acquire data from any of the transducers (LVDTs, pressure transducer and load cells) or strain gages by entering the proper scale factor or gage factor respectively. This software has a variable scanning rate that ranges from 1 to 2500 scans/second with a maximum file size of 2 gigabytes. A scanning rate of 10 scans/second was selected for the test.

2.3.2 Hollow Cylinder rams:

Two double-acting hollow plungers ENERPAC RRH-10010 were also used in conjunction with a self-reacting frame for this third test. The hollow plungers have a maximum stroke range of 10 inches, and maximum load capacity of 206 kips advancing and 136 kips retracting.

2.3.3 Self-Reacting Frame:

A self-reacting frame, sketched in Fig. 5, was used to apply load to the RBX system. It consists of two vertical W12x58 columns and two beams made with MC18x58 sections. The double channels and the columns were connected through 16 bolts at each joint. Fig. 5 shows the self-reacting frame as it was initially sketched during the design stage, although some modifications were made during fabrication as shown in Appendix A.

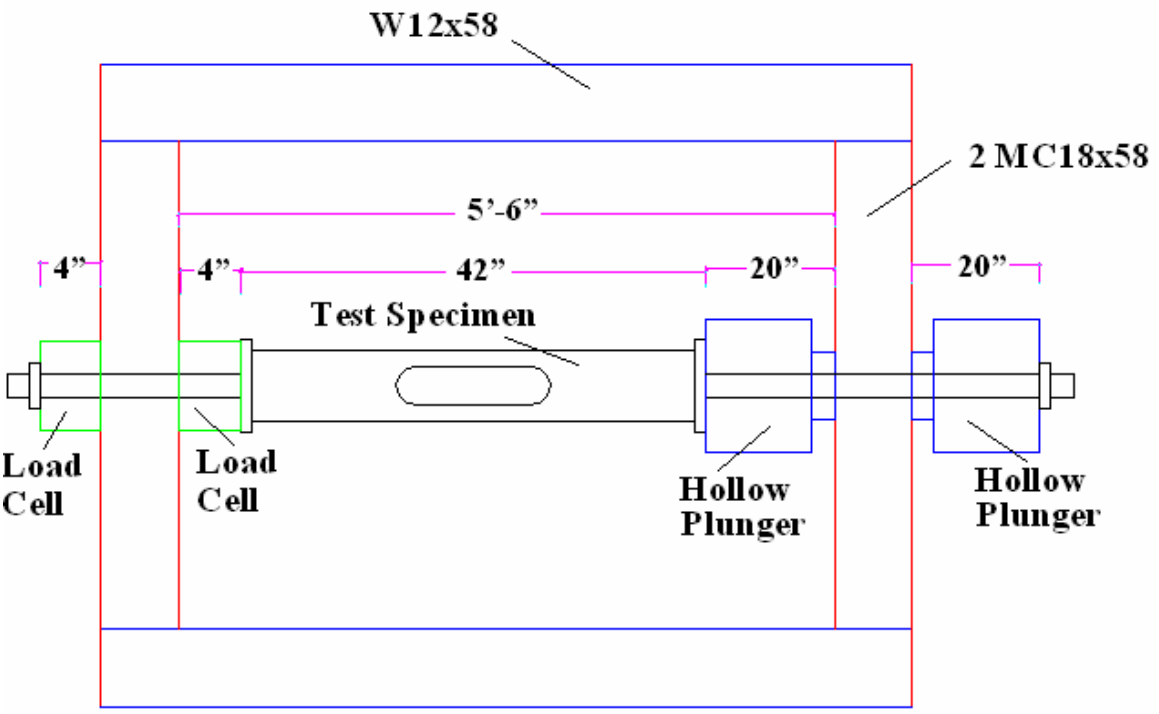

FIG. 5 – SELF-REACTING FRAME SKETCH.

2.4 Loading History

The behavior of test specimens under load reversals is greatly influenced, among other factors, by the displacement history [Tremblay, 2002]. The displacement history that was used in phase 1b, shown in Fig. 6, was a symmetrical displacement pattern devised based on the SAC loading protocol [SAC, 1997] and results from phase 1a (monotonic tests). The loading protocol was designed to provide information concerning the elastic and inelastic behavior of the test specimen under load reversals. The deformation parameter used to control the loading history was the specimen axial deformation divided by the displacement at yield reached by the specimen subjected to monotonic tension.

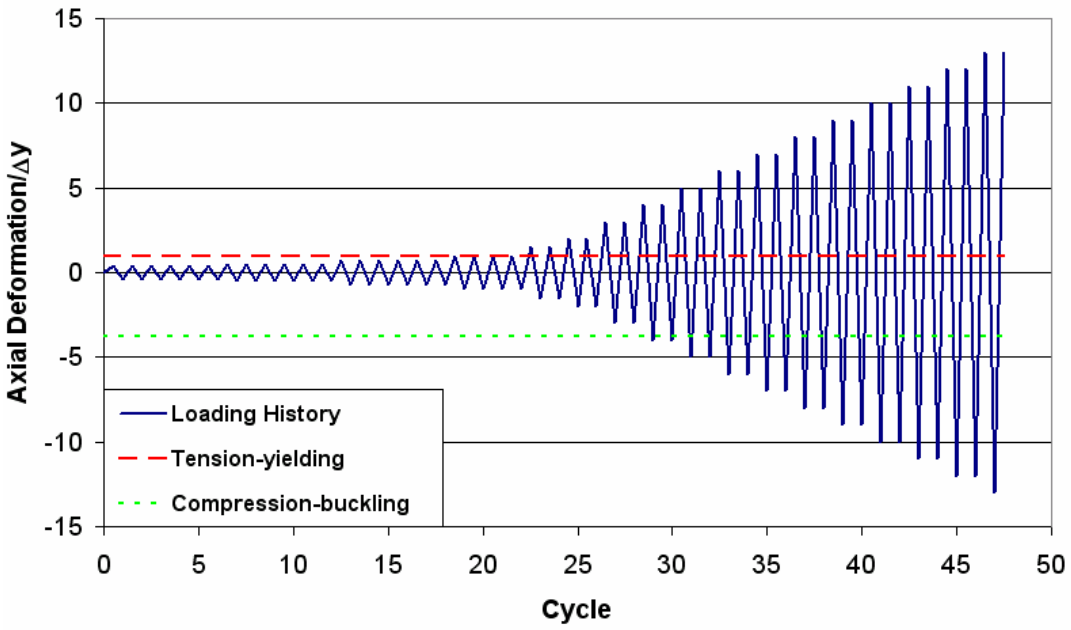

FIG. 6 - LOADING HISTORY.

As can be seen in Fig 6. the amplitude of the displacement cycles of the loading history in tension and compression increased stepwise at every sixth cycle within the linear-elastic range of behavior, every fourth cycle at yielding, and every second cycle after yielding. The red dashed line in Fig. 6 represents the displacement at yield, Δy, reached by the phase 1a monotonic tension test, whereas the dotted green line represents the displacement at critical buckling reached by the monotonic compression test in phase 1a.

The displacement history is summarized in Table 1. Based on results from phase 1a it was anticipated that a maximum of twenty-four load steps and sixty-two cycles would occur before failure. Table 1 shows that at load step twenty-four, which corresponds to cycle sixty-two overall, the specimen would have reached the maximum axial deformation recorded during phase 1a under monotonic tension. Even though the maximum axial deformation could have been higher than that recorded in phase 1a due to

the implementation of bridge fabrication practice with smooth edges, it was assumed that the low cycle fatigue associated with the load reversals would reduce the maximum deformation the specimen could achieve prior to failure due to fracture.

Strain gage (in./in.)								
Load Step #	cycles	Sum:cycles	Peak deformation	%	strain (in./in) **strain gage** control	axial deformation/Δy	Axial displac. **LVDT** (in) control	tension **LOAD** (Lb)
1	6	6	0.00375	37.5	1.13E-03	0.38	0.032	91000
2	6	12	0.005	50	1.50E-03	0.50	0.038	105500
3	6	18	0.0075	75	2.25E-03	0.75	0.049	120000
4	4	22	0.01	100	3.00E-03	1.00	0.058	125750
5	2	24	0.015	150	4.50E-03	1.50	0.074	130600
6	2	26	0.02	200	6.00E-03	2.00	0.089	133300
7	2	28	0.03	300	9.00E-03	3.00	0.120	137000
8	2	30	0.04	400	1.20E-02	4.00	0.151	139700
9	2	32	0.05	500	1.50E-02	5.00	0.181	141800
10	2	34	0.06	600	1.80E-02	6.00	0.212	143700
11	2	36	0.07	700	2.10E-02	7.00	0.242	145400
12	2	38	0.08	800	2.40E-02	8.00	0.272	146880
13	2	40	0.09	900	2.70E-02	9.00	0.303	148200
14	2	42	0.1	1000	3.00E-02	10.00	0.333	149450
15	2	44	0.11	1100	3.30E-02	11.00	0.363	150550
16	2	46	0.12	1200	3.60E-02	12.00	0.394	151570
17	2	48	0.13	1300	3.90E-02	13.00	0.424	152500
18	2	50	0.14	1400	4.20E-02	14.00	0.454	153400
19	2	52	0.15	1500	4.50E-02	15.00	0.484	154200
20	2	54	0.16	1600	4.80E-02	16.00	0.514	155400
21	2	56	0.17	1700	5.10E-02	17.00	0.544	156050
22	2	58	0.18	1800	5.40E-02	18.00	0.575	156650
23	2	60	0.19	1900	5.70E-02	19.00	0.605	157180
24	2	62	0.2	2000	6.00E-02	20.00	0.635	158900
Total cycles	62							
		at tensile yield						
		right before critical buckling						
		maximum buckling deformation during monotonic compression test						
		maximum axial deformation during monotonic tension test before fracture						

TABLE 1 – DISPLACEMENT HISTORY.

Chapter 3 Experimental Results

3.1 Expected Behavior

Based on the behavior of the specimens observed during phase 1a it was expected that the phase 1b specimen would reach the yield deformation in tension after load step #4. Similarly, it was expected that under compressive loads the specimen would reach the critical buckling load after step #5 (Table 1).

After the specimen started to deform in the inelastic range of response in both compression and tension, it was expected that the nominal capacity would deteriorate under load reversals due to two main causes: Bauschinger effect, and the effect of residual curvature resulting from plastic hinge rotations during previous cycles. Furthermore, based on previous experiments from other studies, it was expected that after the critical buckling load was reached the compressive capacity at subsequent cycles would decrease to almost half of the initial critical buckling capacity.

Bauschinger effect: when materials are loaded uniaxially in one direction (e.g. in tension) into the plastic regime, unload to zero stress level, then reloaded in reverse direction (e.g. in compression), they may yield during the reloading, at a stress level lower than if the reloading were carried out in the original direction.

3.2 Observations during test

Deformation control was used throughout the experiment following the devised loading history.

It was observed during the first cycle of the second load step (cycle #7 overall) that one of the RXS three arms started to show buckling deformations. Because it was not expected to have inelastic deformations at such early stages of the loading history, the experiment was interrupted at this point. Upon review of the reaction system it was found that a small eccentricity was being applied towards the arm that buckled, as can be seen in Appendix B. For this reason that arm was subjected to stresses higher than those predicted for the second load step, which caused such early buckling of that particular arm. The other two arms did not show any signs of buckling at this stage of the displacement history. The position of the specimen was adjusted to minimize the eccentricity and the experiment continued with the previously defined displacement history.

Yield deformations were not observed nor recorded by the instrumentation during load step #4. Therefore it was decided to modify the loading history for subsequent load steps from 2 cycles per load step to 4 cycles until yield deformations were recorded. However, inelastic deformations under tension loads were never observed or recorded by the instrumentation during subsequent load steps.

The other two arms that had not initially buckled, started to show inelastic deformations under compressive loads after load step #5. The test continued after verification that the applied load was concentric.

As the test progressed by increasing the displacement at every load step, severe buckling deformations were visually detected under compression. These buckling deformations accentuated with every subsequent cycle. After load step #6 it was observed

that the thin coating of whitewash started to detach from the surface of the RXS, which was a sign of deterioration. This deterioration became more evident as the test continued.

As mentioned above the specimen was never subjected to inelastic deformations under tension loads even at peak displacements. It was observed that at peak displacement under tension the arms never recovered their original straight shape. Instead a residual buckling deformation was observed, but not as severe as the buckling deformation at peak displacement under compression loads.

During the first cycle of load step #12, fifty-first cycle overall, the arm that initially buckled failed due to a horizontal crack located at the middle of inner face of the arm. This crack initiated simultaneously at the center of the two longitudinal cuts, and propagated from the edges of the inner face of the arm inner towards its longitudinal center as load was applied. It was observed that immediately after the crack propagated in the first arm, the other two arms had the same type of failure. The test concluded at load step #12, when failure was visually detected.

3.3 Behavior of the specimen

Figure 7 shows the load-displacement response of the specimen to the loading history up to load step #12 ($\Delta = \pm 8.0\ \Delta y$), when failure occurred.

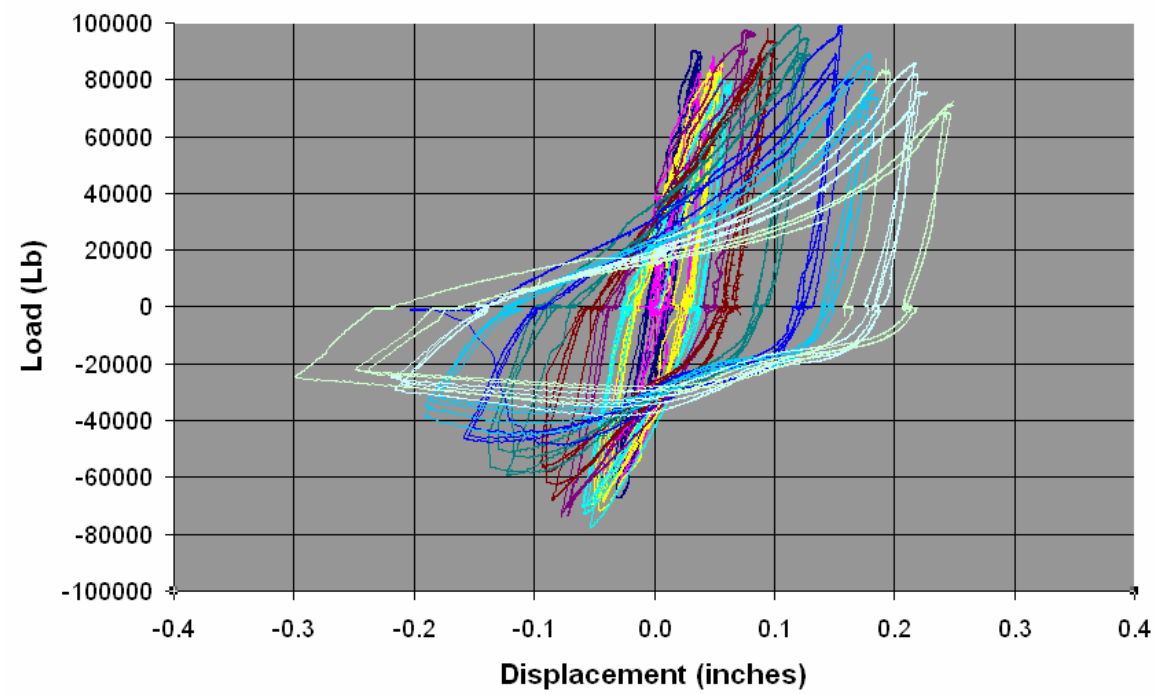

FIG. 7 – AXIAL LOAD VS. DISPLACEMENT RESPONSE

As previously mentioned, under tension loads the specimen never reached the yield deflection of the specimen loaded monotonically in tension, and the maximum tensile force for every load step after the initial buckling deformation took place were well below the nominal capacity of the cross section in tension. Under compression loads the specimen was subjected to inelastic deformations from the very beginning of the test. Even though the maximum compressive loads recorded for each cycle were well below the nominal strength, the specimen was able to withstand buckling deformations for more than 44 cycles prior to failure.

Chapter 4 Conclusions and Recommendations

The difference between the predicted and observed damage levels can be attributed to the eccentricity of the applied axial loads at the beginning of the test. This eccentricity created a non-uniform stress distribution along the reduced brace section. The load-displacement response of the specimen exhibited limited energy dissipation capacity due to the premature buckling of the arms. For this reason, the reduced section could not develop its nominal yield capacity.

The experiment in phase 1b showed that the RXS system was highly sensitive to eccentricities on axial loading, and that those must be accounted for in its design. This can be achieved by either proportioning the cutoffs so that local buckling will not take place under a reasonable level of eccentricity expected to take place in a braced frame, or by reinforcing the reduced section to improve its performance under eccentric loading.

Additional testing could be carried out on similar specimens even with different design properties to obtain more data on the inelastic seismic performance of the RXS. In particular the influence of different loading histories could be carefully examined to ensure that a robust seismic performance, without premature failure, can be achieved. The effect of non-uniform stresses due to eccentricity could be studied by varying the distance between the RXS and the gusset plate connection.

Chapter 5 References

American Institute of Steel Construction, Inc. (AISC). (1999). Load and Resistance Factor Design Specification for Structural Steel Buildings. AISC, Chicago, IL, December 27.

American Institute of Steel Construction, Inc. (AISC). (1997). Hollow Structural Sections (HSS) Connections Manual, AISC, Chicago, IL.

American Institute of Steel Construction, Inc. (AISC) (1997), Seismic Provisions for Structural Steel Buildings, AISC, Chicago, IL.

American Institute of Steel Construction, Inc. (AISC) (2002), Seismic Provisions for Structural Steel Buildings, AISC, Chicago, IL.

American Society for Testing and Materials (ASTM). (2003). Annual Book of ASTM Standards, Metals Test Methods and Analytical Procedures. Section 3, Vol. 3.01, West Conshohocken, Pennsylvania.

SAC. (1994). Analytical and Field Investigations of Buildings affected by the Northridge earthquake of January 1994. SAC 9504 Part 1 & 2, SAC Joint Venture, Sacramento, CA.

SAC. (1997). Protocol for fabrication, inspection, testing and documentation of beam-column connection tests and other experimental specimens. Report No. SAC/BD-97/02, SAC Joint Venture, Sacramento, CA.

Salmon, Charles G., and Johnson, John E. (1996). Steel Structures: Design and Behavior, Emphasizing Load and Resistance Factor Design. Fourth Edition, Harper Collins, Inc., New York.

Segui, W. T. (2003). LRFD Steel Design. Third Edition. Brooks/Cole-Thomson Learning, Pacific Grove, CA.

Tremblay, R. (2002). Inelastic seismic response of steel bracing members. Journal of constructional steel research, volume 28, number 5-8, pages 665-701.

Appendix A – Experimental Configuration

FIG. A1 – TEST SET-UP PHOTO; REACTING FRAME.

Appendix B – Load Step #2

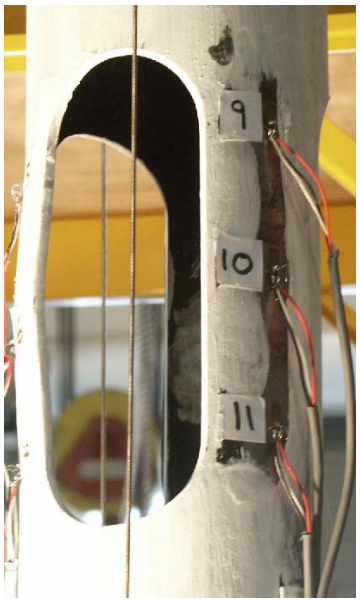

FIG. B1- INITIAL BUCKLING DEFORMATION AT ONE ARM; LOAD STEP #2 FIRST CYCLE.

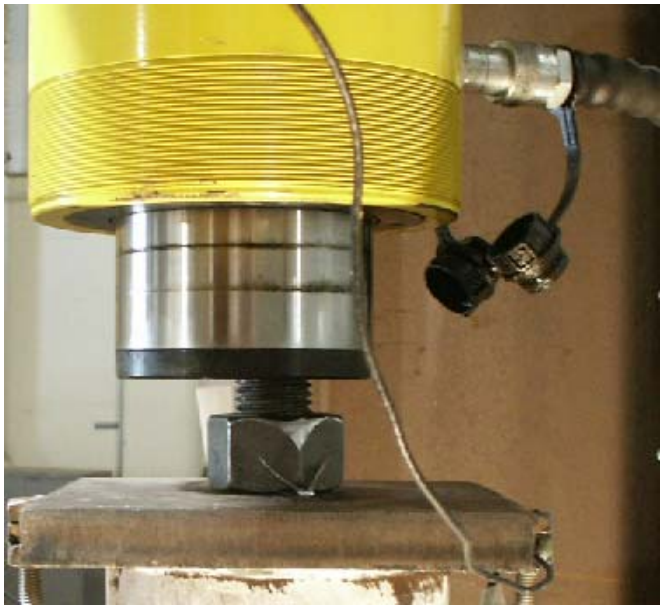

FIG. B2 - INITIAL ECCENTRICITY.

FIG. B3 – BUCKLING DEFORMATION; LOAD STEP #2 LAST CYCLE.

Appendix C – Load Step #4

FIG. C1 – BUCKLING DEFORMATION; LOAD STEP #4 LAST CYCLE.

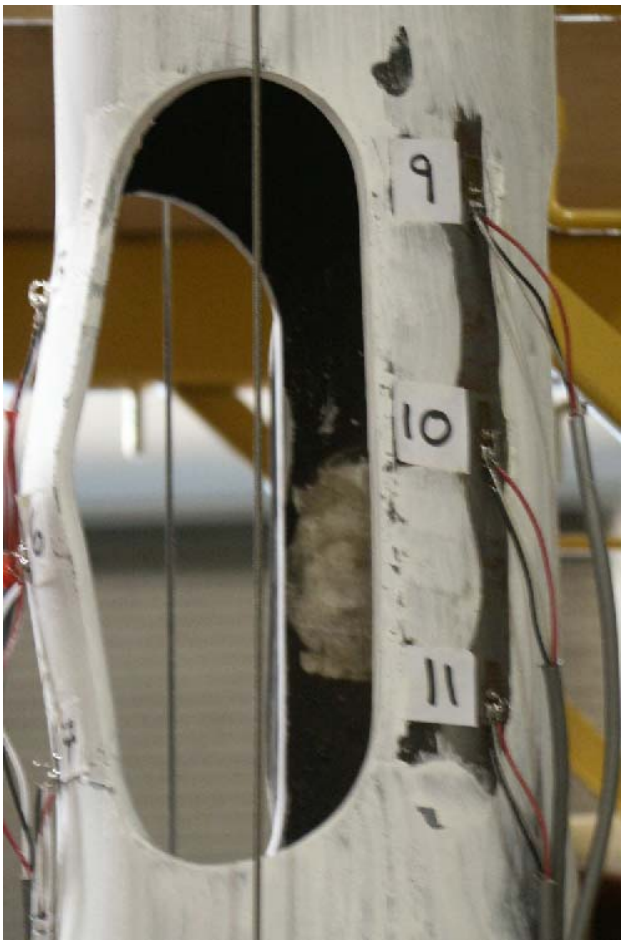

FIG. C2 – BUCKLING DEFORMATION CLOSE-UP; LOAD STEP #4 LAST CYCLE.

Appendix D – Load Step #6

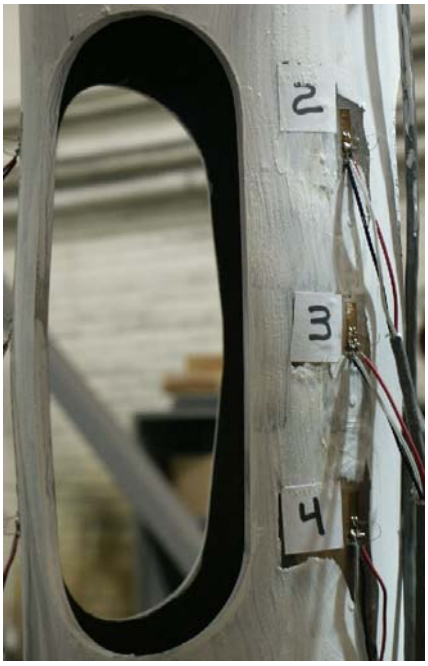

FIG. D1 – INITIAL BUCKLING DEFORMATIONS AT OTHER TWO ARMS LOAD STEP #6.

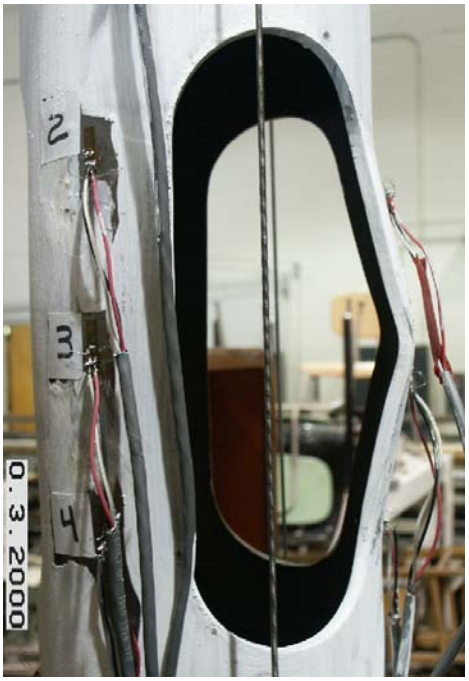

FIG. D2 – FIRST ARM THAT BUCKLED, PEAK COMPRESSION DISPLACEMENT LOAD STEP #6.

Appendix E – Load Step #8

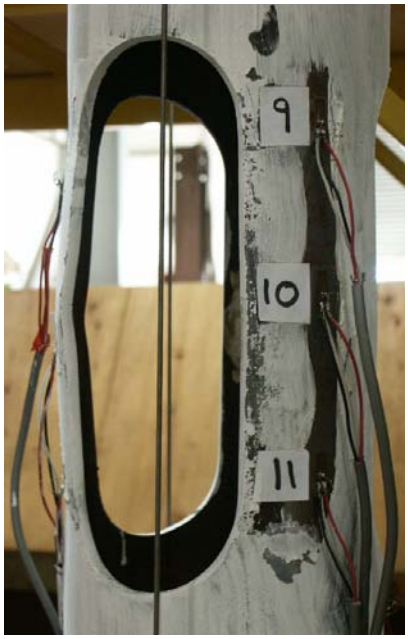

FIG. E1 – PEAK DEFORMATION UNDER TENSION LOAD; LOAD STEP #8 LAST CYCLE.

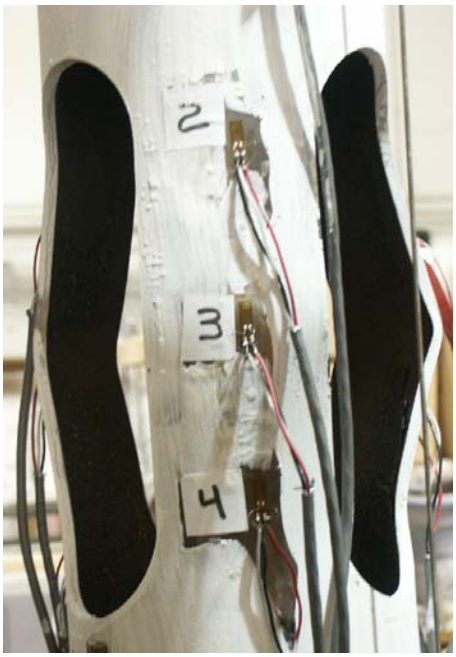

FIG. E2 – PEAK DEFORMATION UNDER COMPRESSION LOAD; LOAD STEP #8 LAST CYCLE.

Appendix F – Load Step #9

FIG. F1 - PEAK DEFORMATION UNDER TENSION LOAD; LOAD STEP #9 LAST CYCLE.

FIG. F2 - PEAK DEFORMATION UNDER COMPRESSION LOAD; LOAD STEP #9 LAST CYCLE.

Appendix G – Load Step #10

FIG. G1 - PEAK DEFORMATION UNDER TENSION LOAD; LOAD STEP #10 LAST CYCLE.

FIG. G2 - PEAK DEFORMATION UNDER COMPRESSION LOAD; LOAD STEP #10 LAST CYCLE.

Appendix H – Load Step #11

FIG. H1 - PEAK DEFORMATION UNDER TENSION LOAD; LOAD STEP #11 LAST CYCLE.

FIG. H2 - PEAK DEFORMATION UNDER COMPRESSION LOAD; LOAD STEP #11 LAST CYCLE.

Appendix I – Load Step #12

FIG. I1 – FATIGUE FAILURE, LOAD STEP #12, FIRST CYCLE.

FIG. I2 – FATIGUE FAILURE CLOSE-UP FROM OUTSIDE, LOAD STEP #12, FIRST CYCLE.

FIG. I3 – FATIGUE FAILURE FROM INSIDE, LOAD STEP #12, FIRST CYCLE.

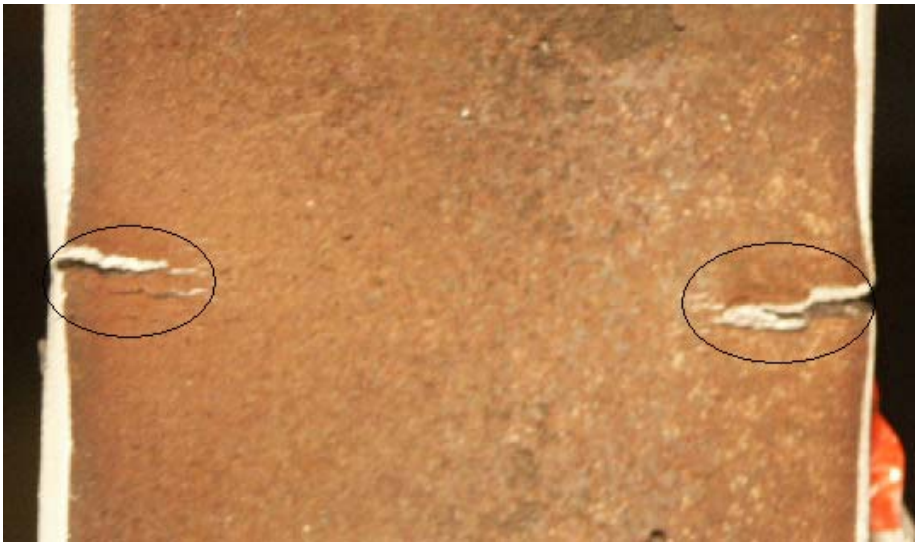

FIG. I4 – FATIGUE FAILURE CLOSE-UP FROM INSIDE, LOAD STEP #12, FIRST CYCLE.

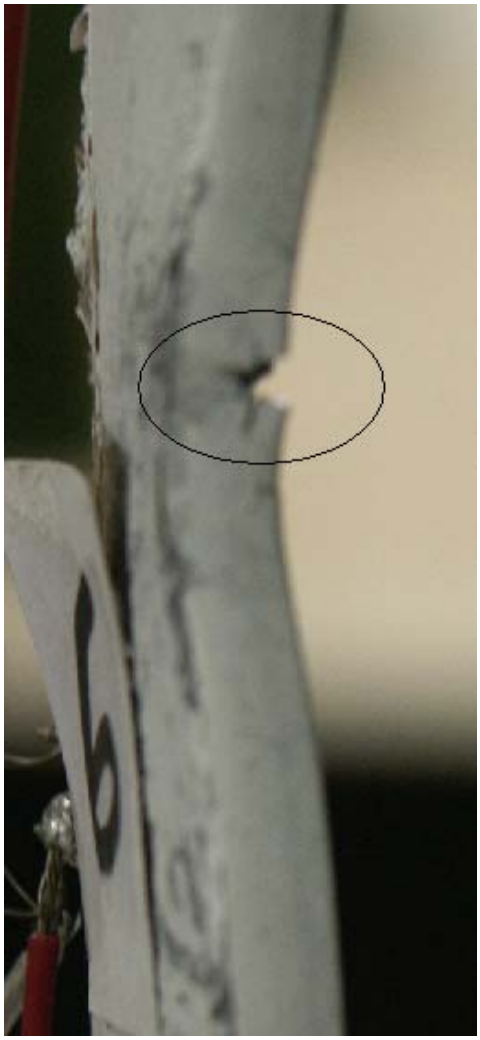

FIG. I5 – FATIGUE FAILURE CLOSE-UP FROM SIDE, LOAD STEP #12, FIRST CYCLE.

Appendix J – Axial Load vs. Displacement Response

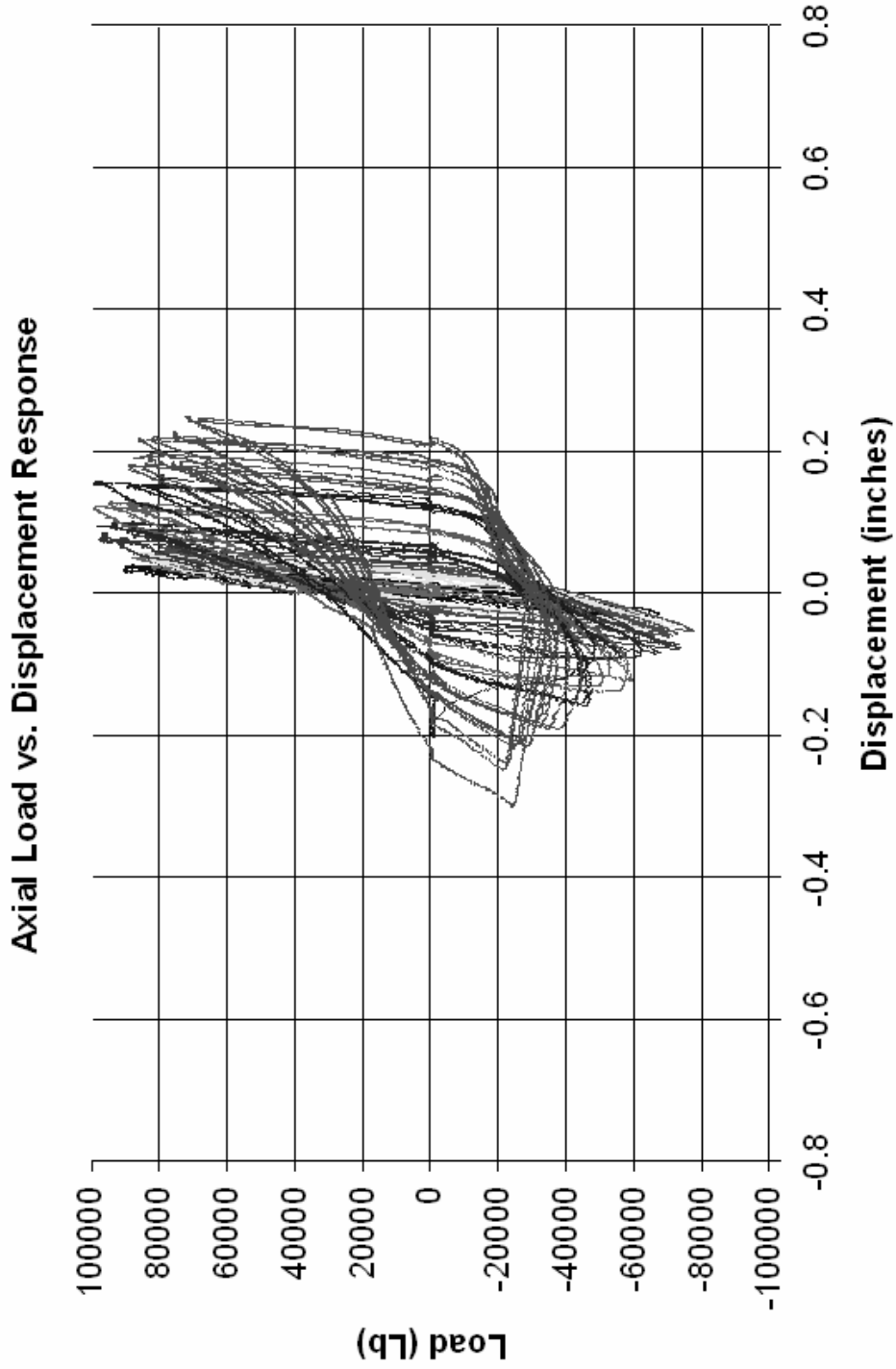

FIG. J1 – AXIAL LOAD VS. DISPLACEMENT RESPONSE; ALL LOAD STEPS.

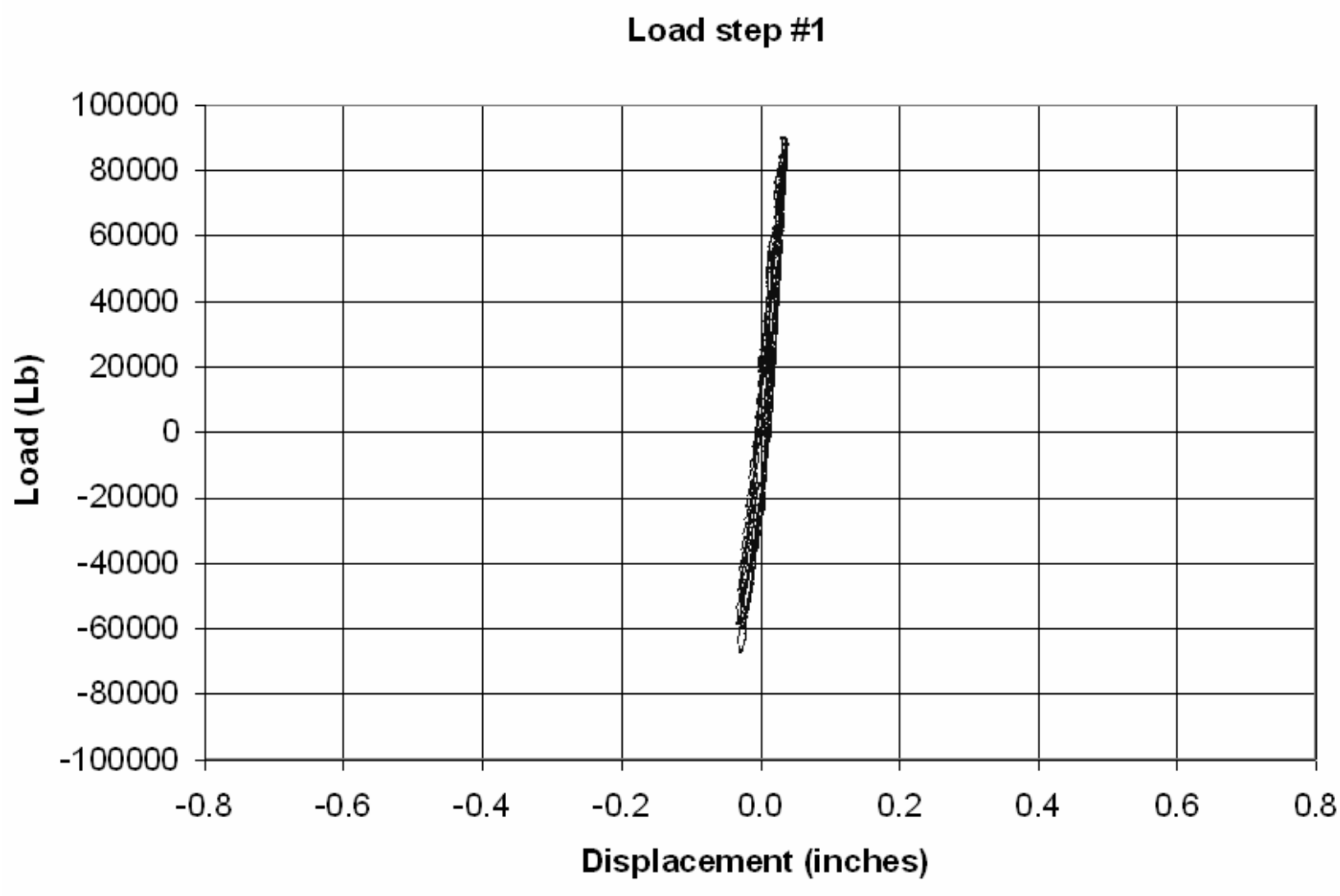

FIG. J2 – AXIAL LOAD VS. DISPLACEMENT RESPONSE; LOAD STEP #1.

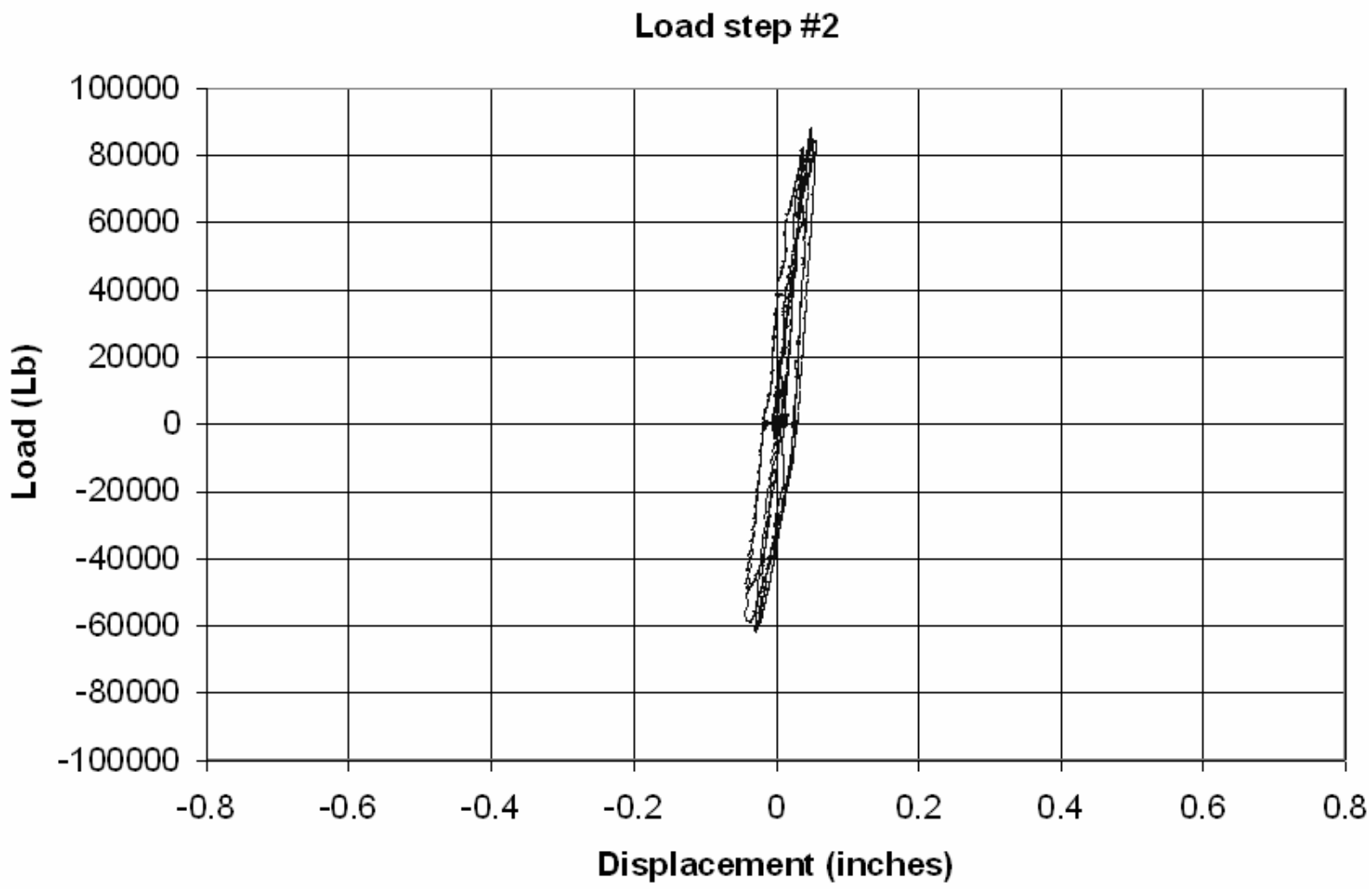

FIG. J3 – AXIAL LOAD VS. DISPLACEMENT RESPONSE; LOAD STEP #2.

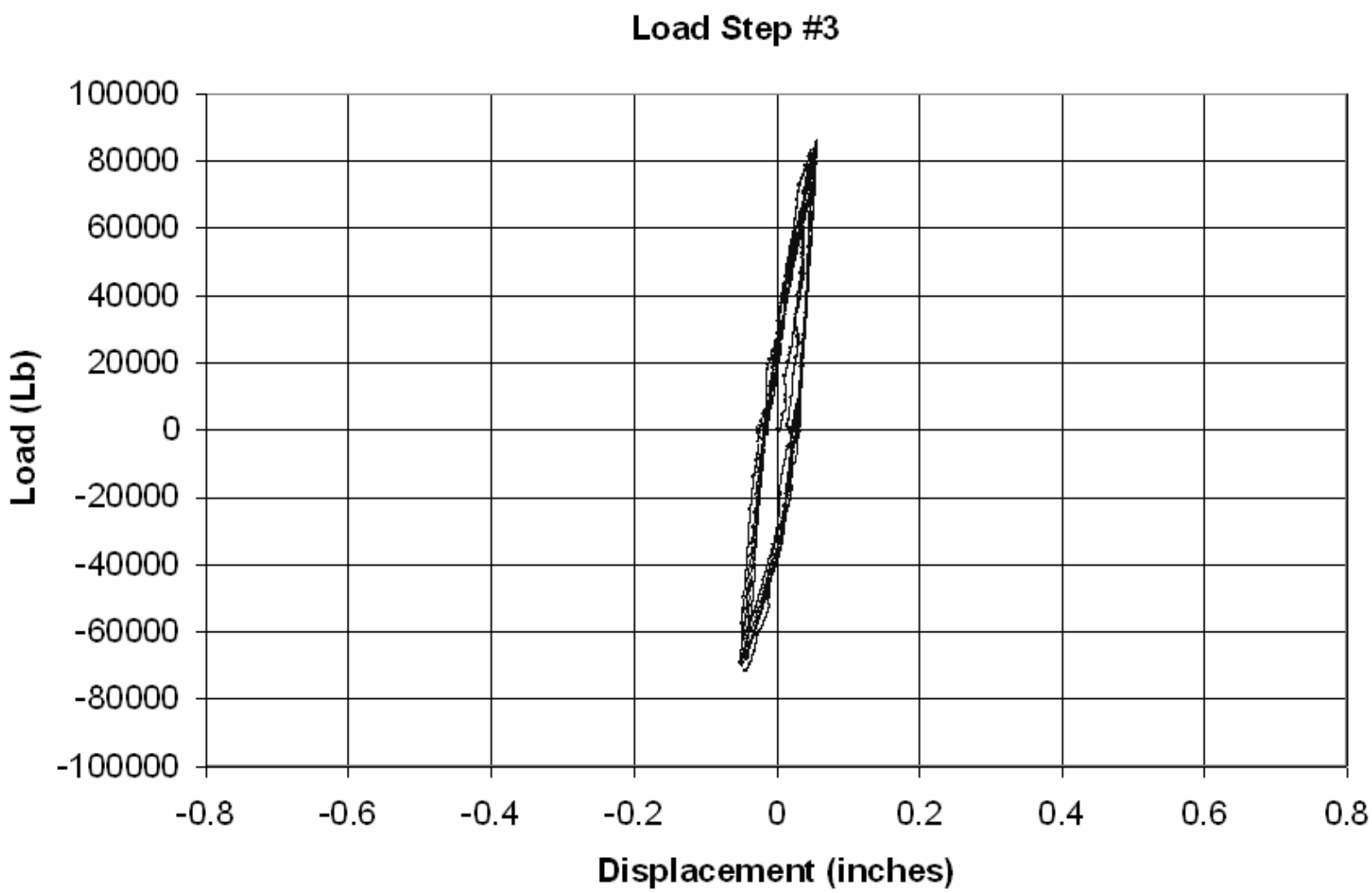

FIG. J4 – AXIAL LOAD VS. DISPLACEMENT RESPONSE; LOAD STEP #3.

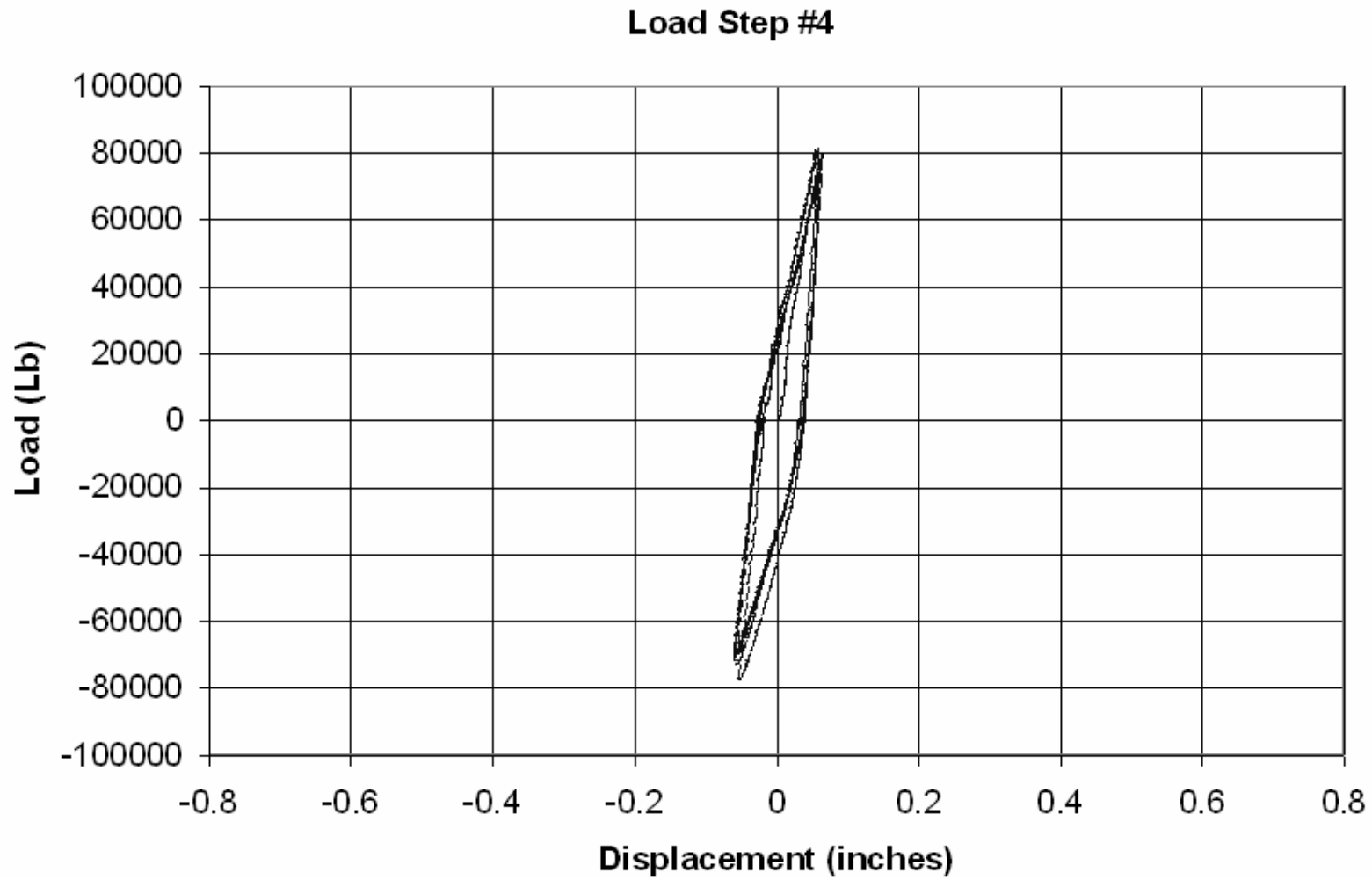

FIG. J5 – AXIAL LOAD VS. DISPLACEMENT RESPONSE; LOAD STEP #4.

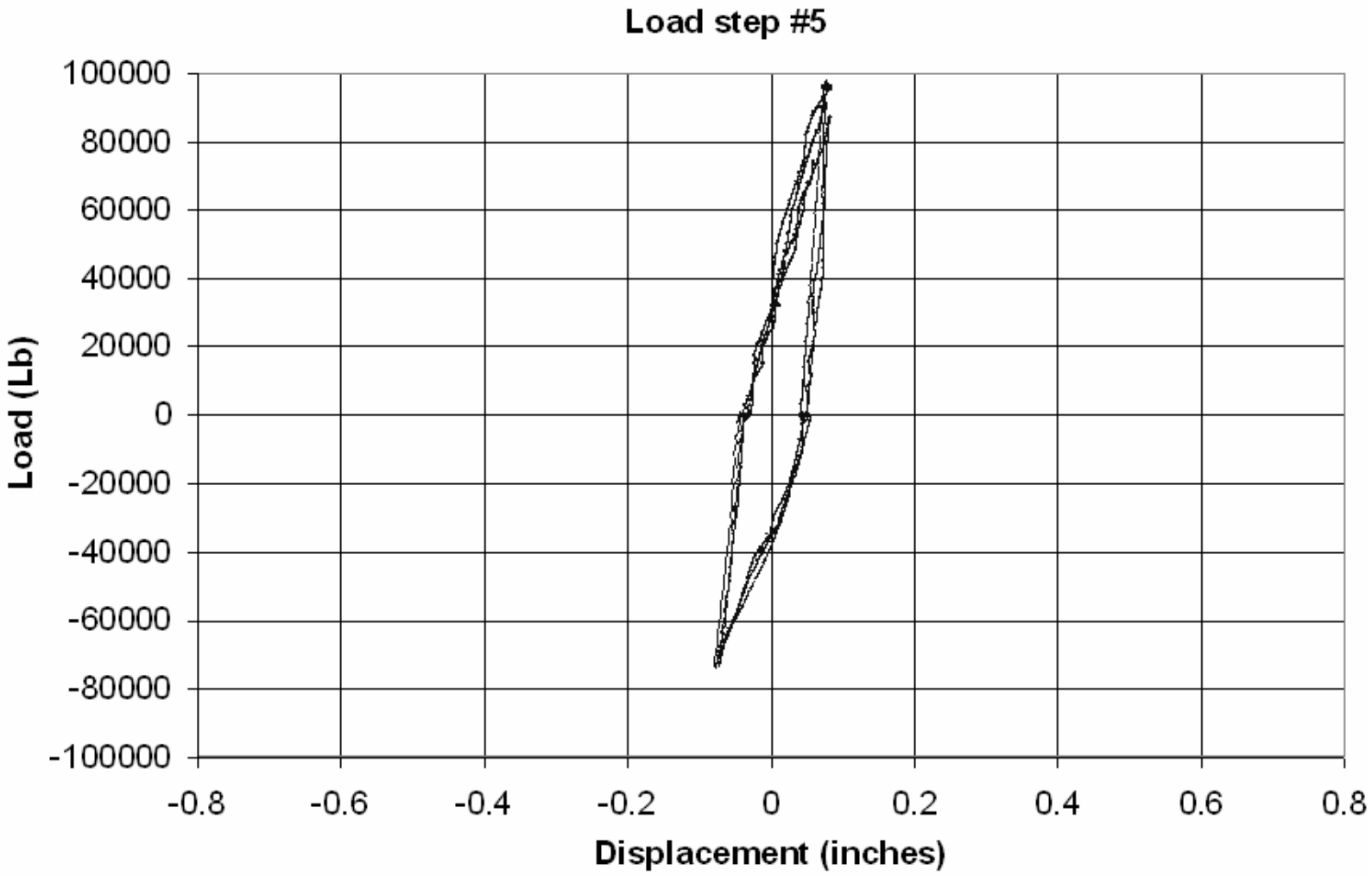

FIG. J6 – AXIAL LOAD VS. DISPLACEMENT RESPONSE; LOAD STEP #5.

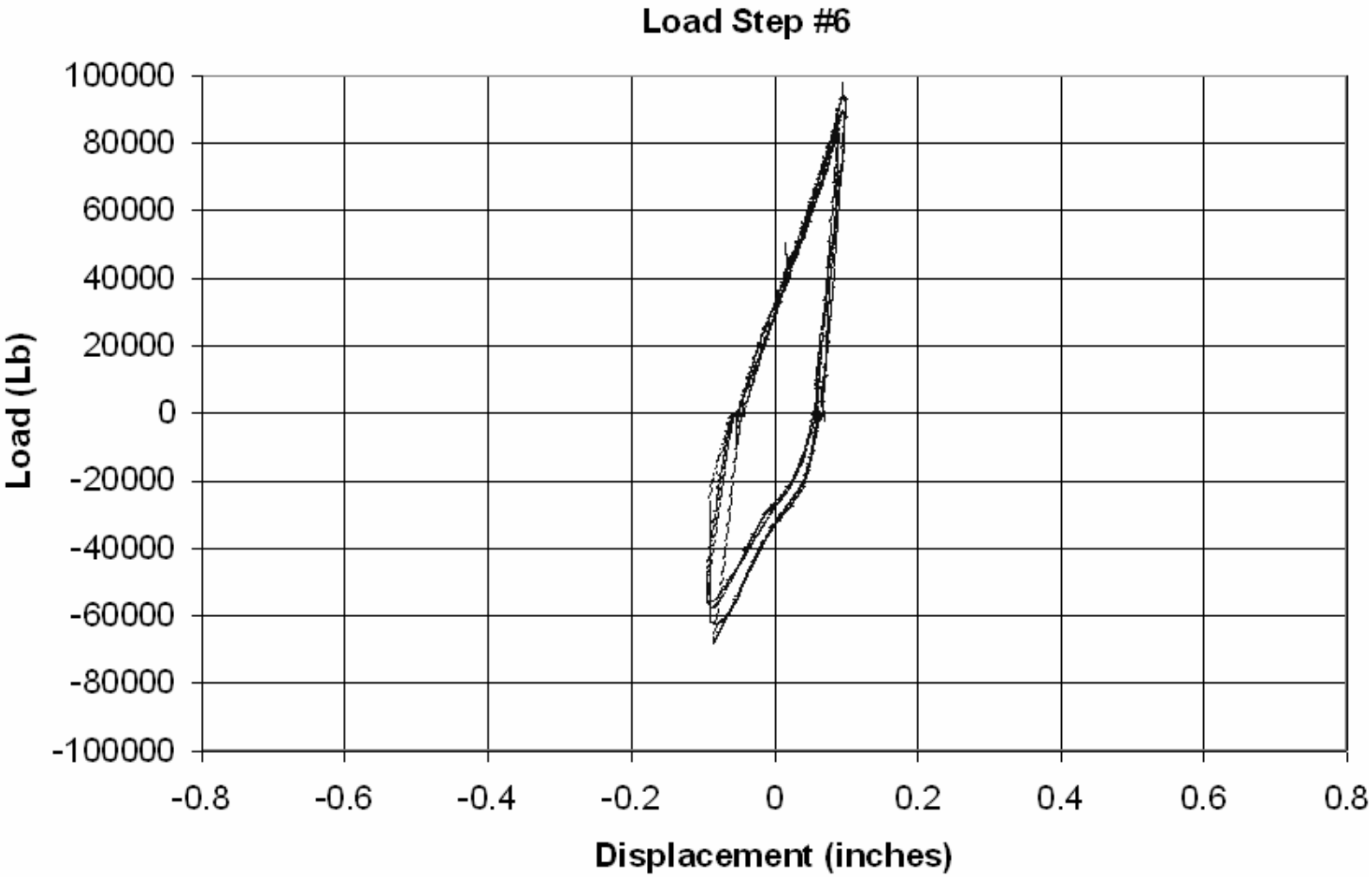

FIG. J7 – AXIAL LOAD VS. DISPLACEMENT RESPONSE; LOAD STEP #6.

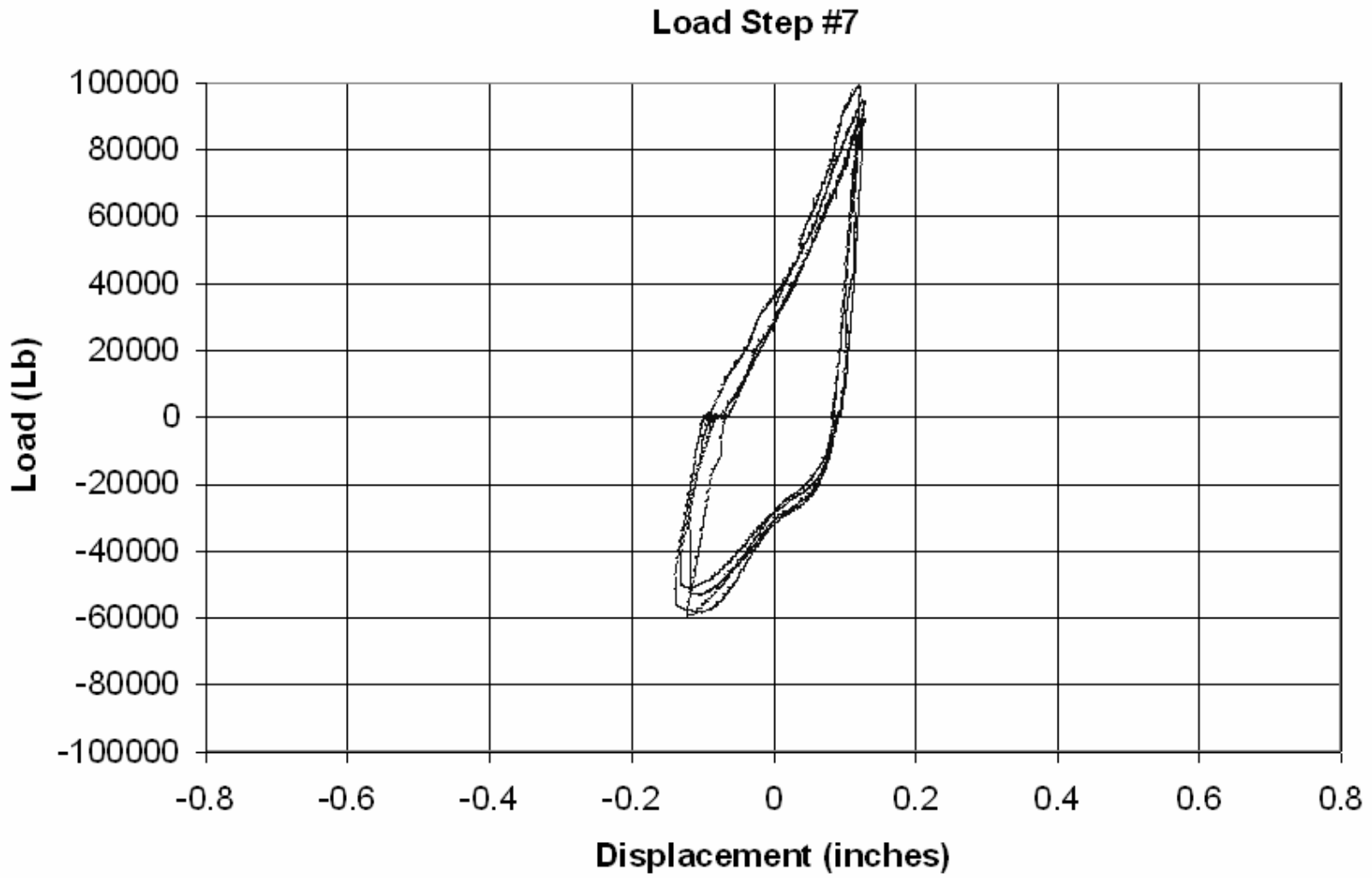

FIG. J8 – AXIAL LOAD VS. DISPLACEMENT RESPONSE; LOAD STEP #7.

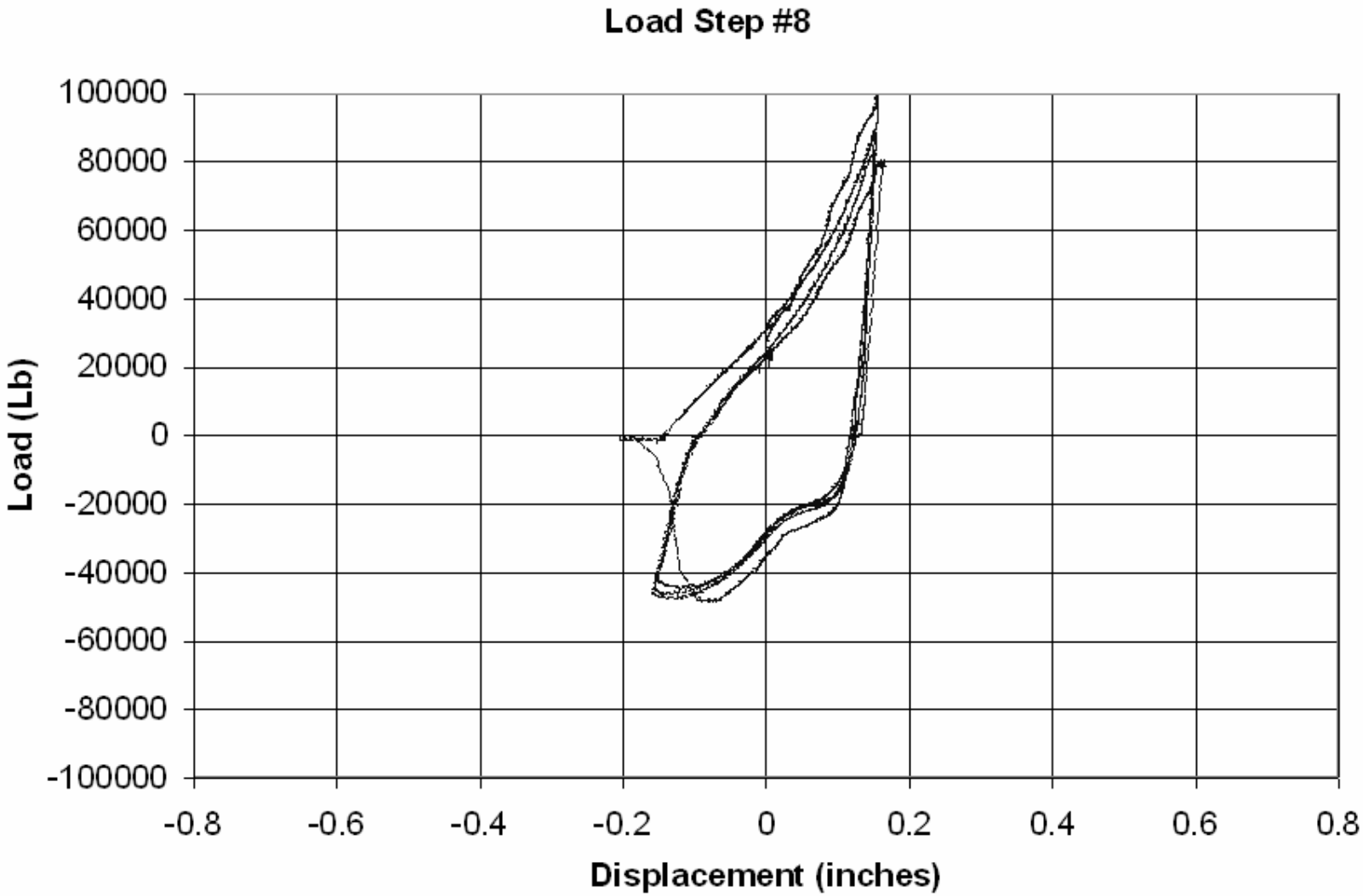

FIG. J9 – AXIAL LOAD VS. DISPLACEMENT RESPONSE; LOAD STEP #8.

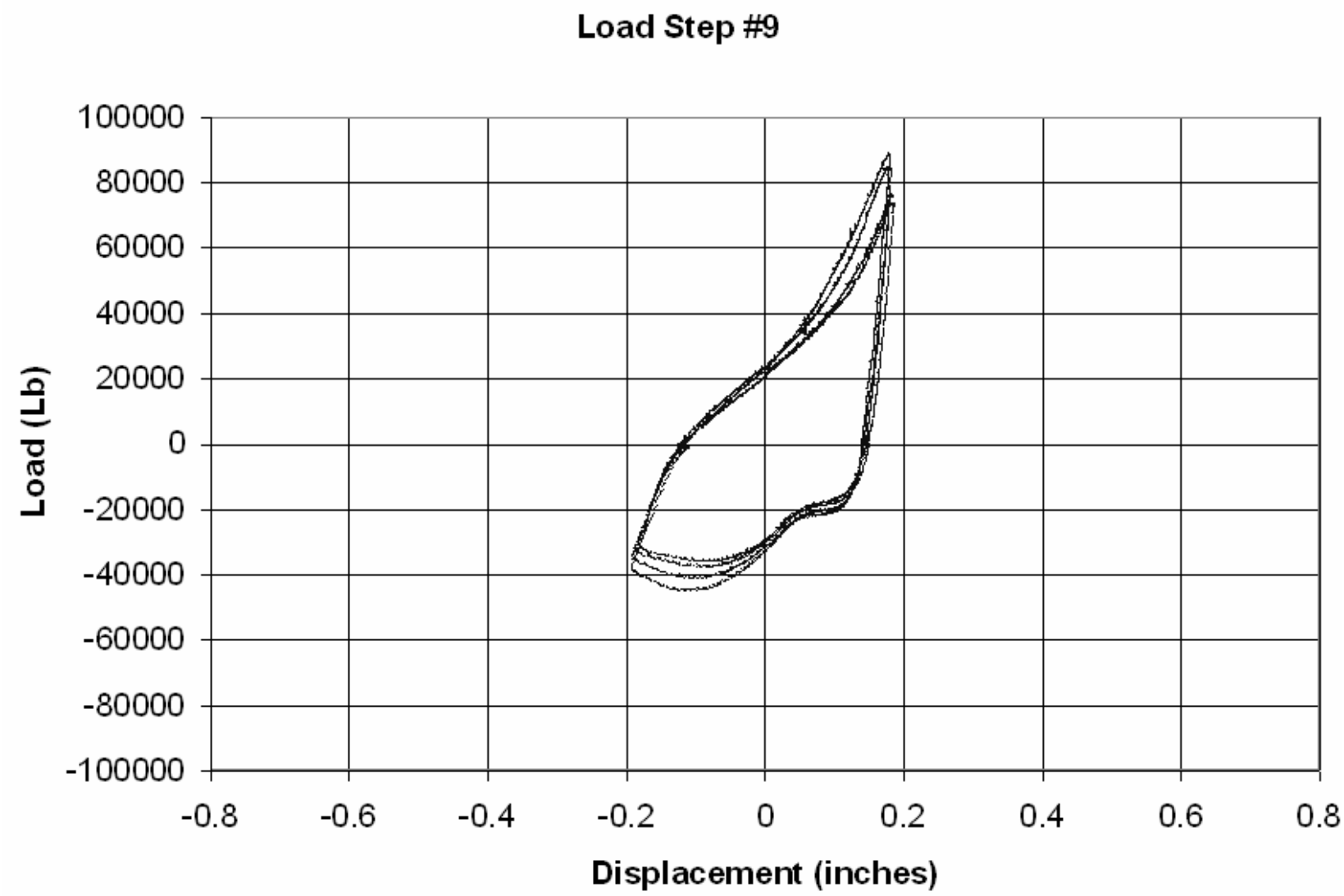

FIG. J10 – AXIAL LOAD VS. DISPLACEMENT RESPONSE; LOAD STEP #9.

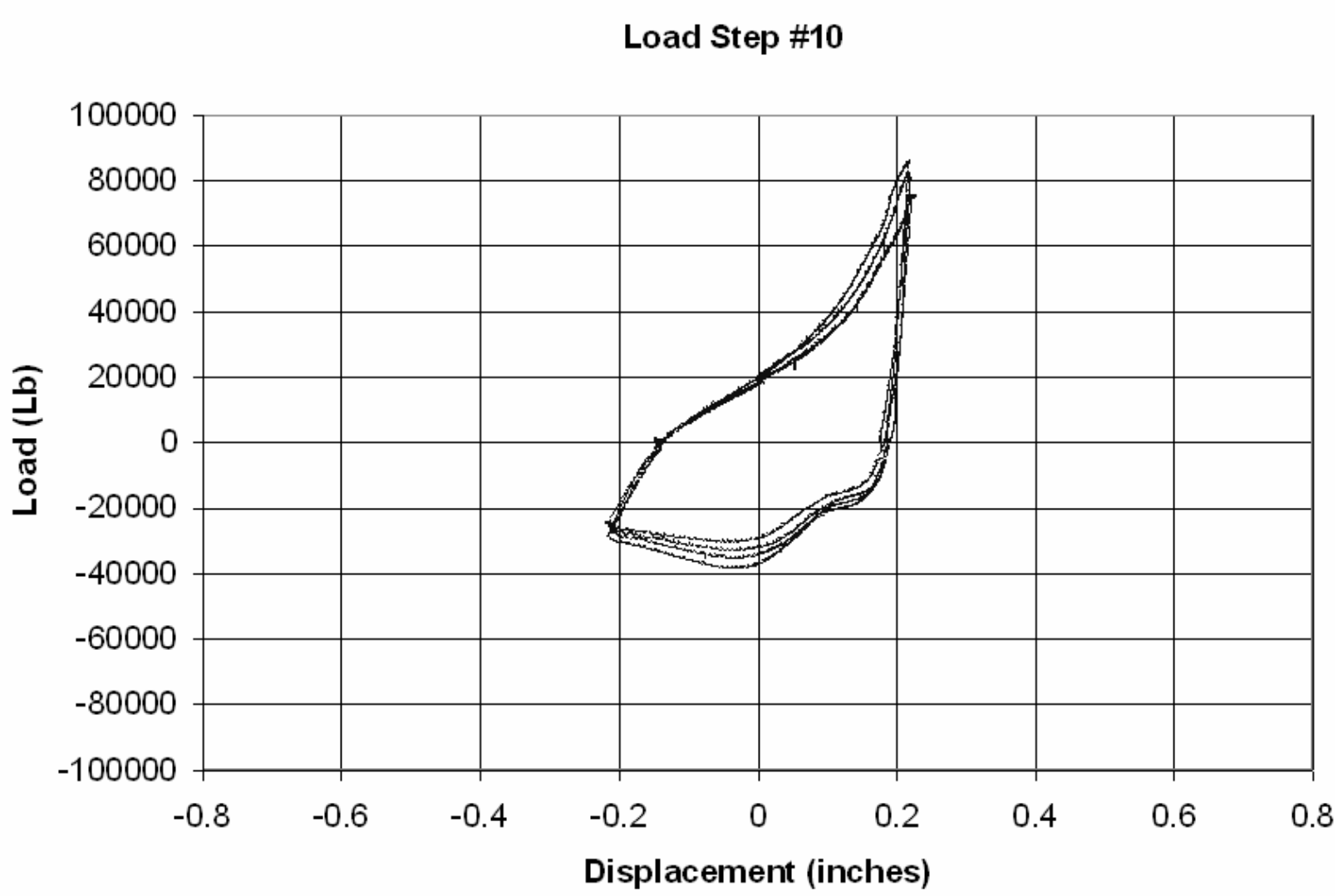

FIG. J11 – AXIAL LOAD VS. DISPLACEMENT RESPONSE; LOAD STEP #10.

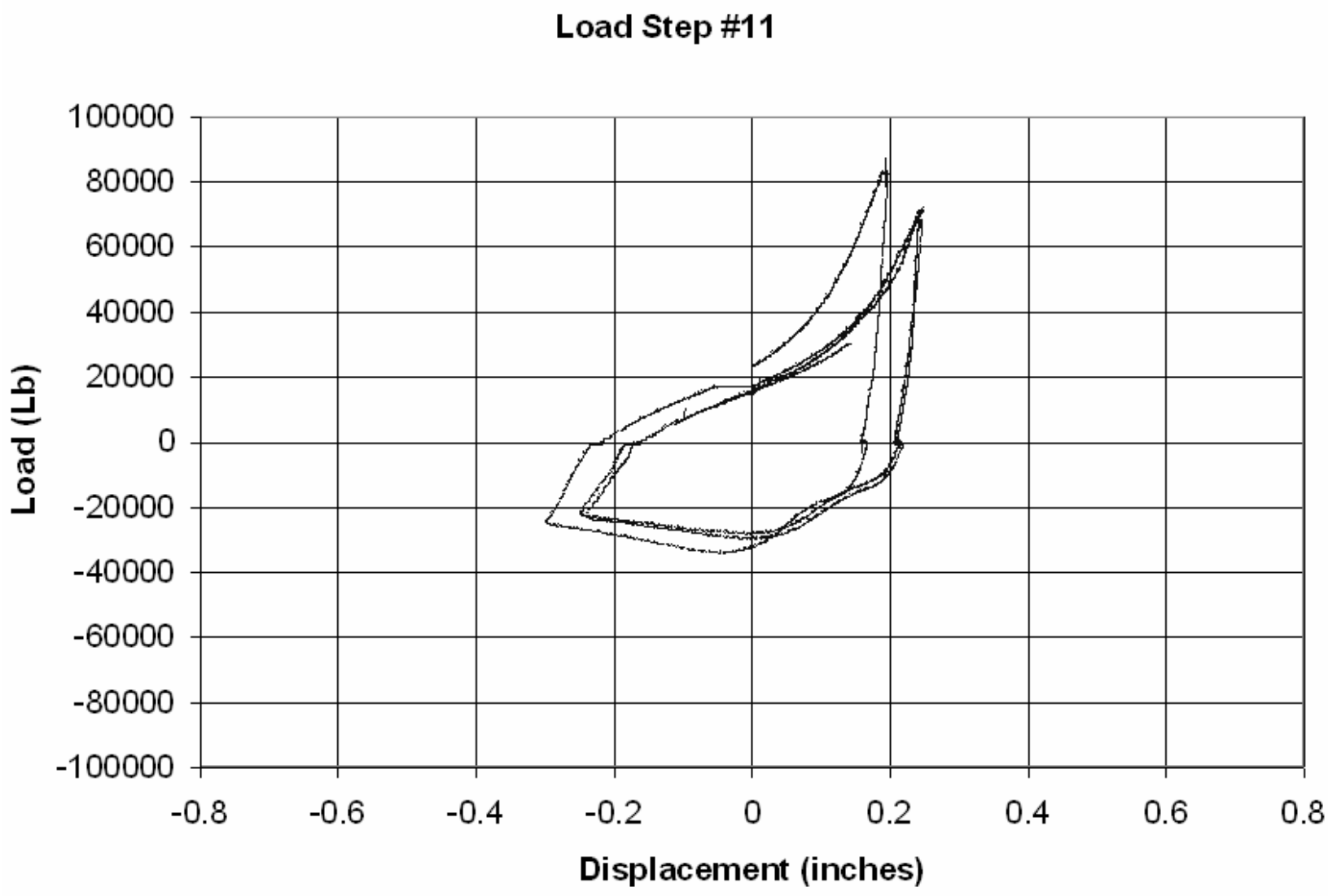

FIG. J12 – AXIAL LOAD VS. DISPLACEMENT RESPONSE; LOAD STEP #11.

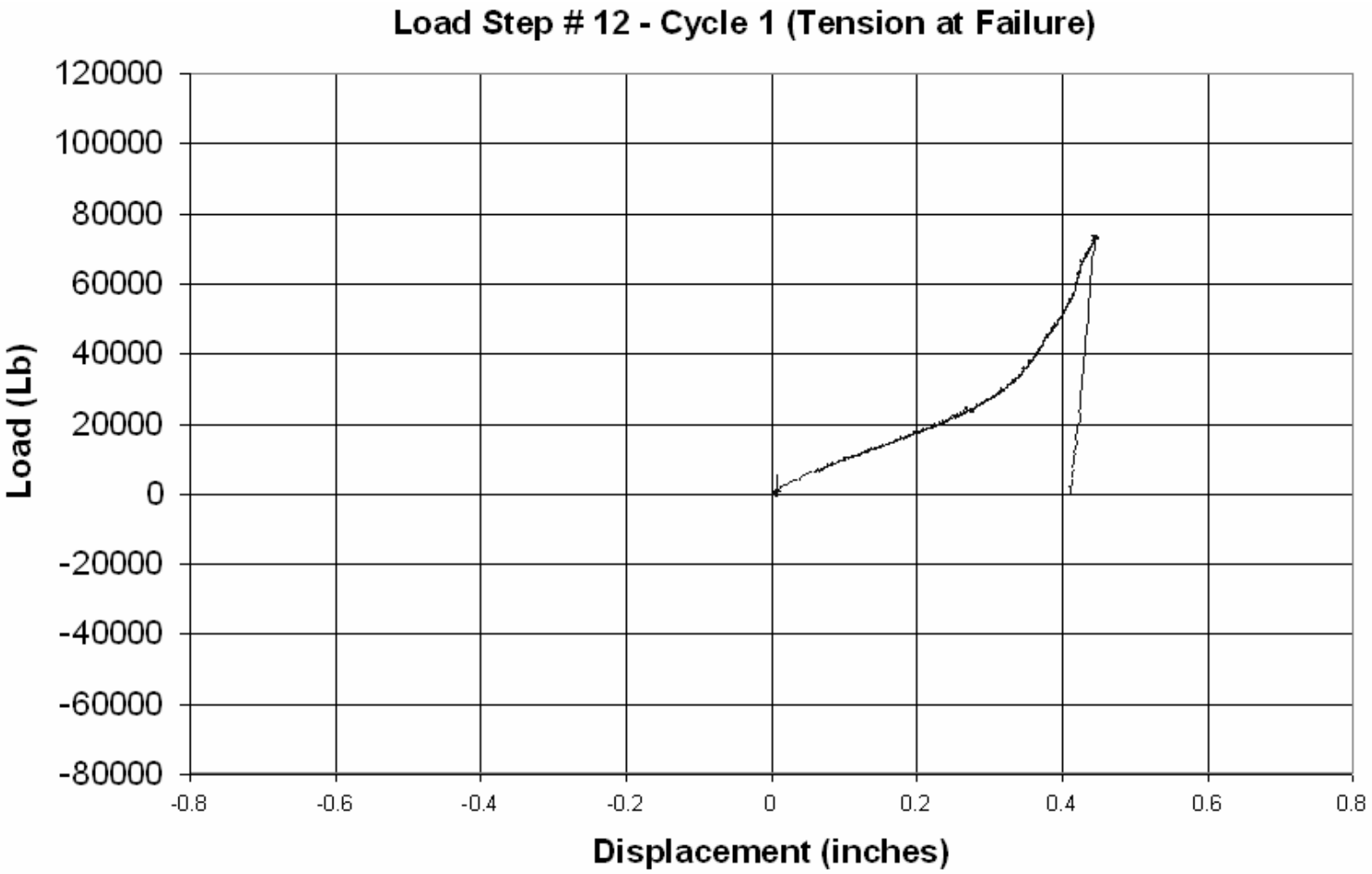

FIG. J13 – AXIAL LOAD VS. DISPLACEMENT RESPONSE; LOAD STEP #12.